Eighth International Conference on
THIN-WALLED STRUCTURES – ICTWS 2018
Lisbon, Portugal, July 24-27, 2018

MODELING AND PERFORMANCE OF THIN-WALLED STEEL DECK IN ROOF DIAPHRAGMS UNDER SEISMIC DEMANDS

Benjamin W. Schafer,[*,] Brooks H. Smith,[**] Shahab Torabian,[*,**] Vahid Meimand[**], and Matt R. Eatherton[***]**

* Johns Hopkins University, USA
e-mail: schafer@jhu.edu

** NBM Technologies, Inc., USA
e-mails: brooks.smith@nbmtech.com, shtorabian@nbmtech.com, vahidzm@nbmtech.com

** Virginia Polytechnic and State University., USA
e-mail: meather@vt.edu

Keywords: Thin-walled deck, bare steel deck, rigid-wall flexible-diaphragm, inelastic diaphragms.

Abstract. *The objective of this paper is to discuss new models used to predict the seismic performance of large warehouse buildings that employ bare thin-walled profiled steel deck panels as the primary diaphragm element. Warehouse and similar buildings that use tilt-up concrete walls and steel deck supported by open web steel joists, typically resting on HSS columns, are a class of Rigid Wall Flexible Diaphragm (RWFD) buildings. In North America the seismic design of such RWFD buildings has come under question and new methods have been proposed. The nonlinear behavior of the thin-walled steel deck in shear combined with additional nonlinearity between deck-to-deck connections and deck-to-structural connections that form the complete roof diaphragm creates a unique system with unusual energy dissipating mechanisms. A multi-scale model of RWFD buildings has recently been created and exercised under nonlinear time history analyses. Beyond revealing fundamental behavior, the intent of the RWFD modeling work is to provide an evaluation of existing design and newly proposed alternatives for design in North America - an effort that is currently ongoing.*

1 INTRODUCTION

Rigid Wall Flexible Diaphragm (RWFD) buildings are a unique class of structure which combines stiff, often heavy and compact, vertical elements (walls) with light, often thin-walled, horizontal elements (roof diaphragms), as shown in Figure 1. RWFD buildings potentially have unique seismic response since the mass, stiffness, and ductility are all distributed differently than in common building construction. Many warehouses may be classified as RWFD buildings, thus large economic exposure potentially exists when RWFD buildings experience seismic events.

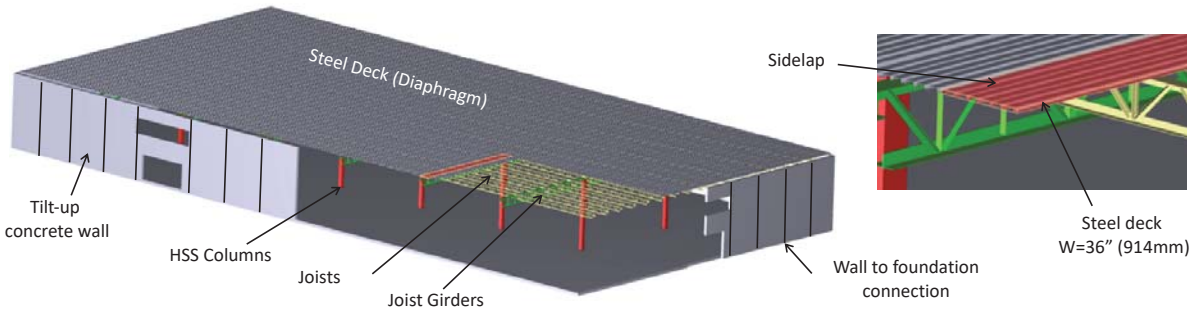

Figure 1: Typical RWFD steel deck diaphragm building

The seismic behavior of RWFD buildings designed to U.S. standards has recently seen comprehensive study. Current designs were evaluated [1] and a new procedure proposed in technical journals [2] and as a resource document from a U.S. agency: FEMA P-1026 [3]. The role of connectors between the roof diaphragm elements was found to be critical and related data for wood and steel deck roof diaphragm connectors collected and organized [4]. A comprehensive, non-linear, two-dimensional model was developed to study RWFD building response. Complete details are provided in [1,2,5] and in the recommended design procedures [3]. Ultimately the researchers expressed hesitation with finalizing recommendations for steel deck diaphragms in RWFD buildings due to a lack of comprehensive connector data, concern over whether limit states observed in testing were fully captured in the modeling, and other practical issues as detailed in [3]. The lack of connector data largely reflects the fact that (a) industry has traditionally conducted cantilever diaphragm tests instead of individual connector tests, and (b) most existing data is monotonic. A recent summary of available steel deck diaphragm tests is available [6].

Prior work in Canada on seismic performance of steel deck diaphragms indicated limitations when employed in RWFD buildings [7]. Steel connectors for both deck-to-deck (sidelap) and deck-to-frame (structural) were studied cyclically in shear [8,9]; relatively large out-of-plane movements occurred in the test specimens. Static and quasi-static testing demonstrated challenges with developing large amounts of ductility in conventionally detailed steel deck diaphragms [10]. Details were developed that provide a means for welded and fastened steel deck diaphragms to achieve increased ductility, but ultimately it was concluded for Canadian design to recommend elastic diaphragm designs in RWFD buildings [11].

Given a lack of clear guidance on steel deck diaphragms in RWFD buildings and an interest in understanding the behavior more completely the authors engaged in a study to determine if three-dimensional building models could provide useful predictions of the seismic response and inform design. Bare steel deck diaphragms have at least three key sources of nonlinearity in their in-plane shear response: connector non-linearity, deck material nonlinearity, and due to the use of thin-walled deck geometric nonlinearity of the profiles. A hypothesis of this work was that models incorporating all sources of steel deck diaphragm nonlinearity incorporated in fully three-dimensional building models would have the best opportunity to provide predictions of full building performance.

2 EXAMPLE U.S. RWFD SEISMIC BUILDING DESIGN

Seismic design of RWFD buildings generally follows static Equivalent Lateral Force (ELF) design methods. Critical in this method is accounting for ductility and overstrength through the use of the seismic response modification coefficient, e.g., *R*. Currently, in the U.S. (per ASCE 7-16 [12]), *R* is based solely on the vertical lateral force resisting system – even if inelasticity is expected in the horizontal lateral force resisting system (diaphragm). In ASCE 7 the diaphragm is designed for the mass tributary to the roof, at a spectral acceleration determined from the approximate building period, reduced by *R*, but bounded between empirical limits. To evaluate this design procedure Koliou et al. [1,3,5] developed a series of building archetypes for both wood sheathed and steel deck RWFD buildings.

Koliou et al.'s large building archetype was selected for additional study here and the roof details re-designed based on (a) newly available fastener-data, and (b) input from industry (see acknowledgments) resulting in the building design summarized in Figure 2. The roof uses 38 mm (1.5 in.) deep B deck connected to the structure with Power Actuated Fasteners and connected between deck at the sidelaps with #12 or #10 fasteners. The roof is split into zones employing 18 gauge, 20 gauge, and 22 gauge deck. The design choices reflect a desire

to create a non-proprietary example, and utilize design parameters (deck gauge, fastener type etc.) that we intend to test. (Note, in the short direction the interior zone is adequate for the demands and additional zones are not required).

Aligned with the Koliou et al. design the building is 61 m x 122m (200 ft x 400 ft) in plan, demands are determined per ASCE 7-10 [13] and capacity per AISI S310 [14] (for the steel) and ACI 318 [15] (for the concrete). The concrete tilt up walls are 10 m (33 ft) high with the roof at 9.1 m (30 ft) and a thickness of 234 mm (9.25 in.). Bay spacing is on ~15 m (50 ft) modules, the building is designed for high seismic demands (SDC D, soil class D). Seismic response modification coefficients of R=4, Ω_o=2.5, and C_d=4 are used in the design. The standard period approximation in ASCE 7-10 is employed resulting in a predicted building period of 0.26 sec.

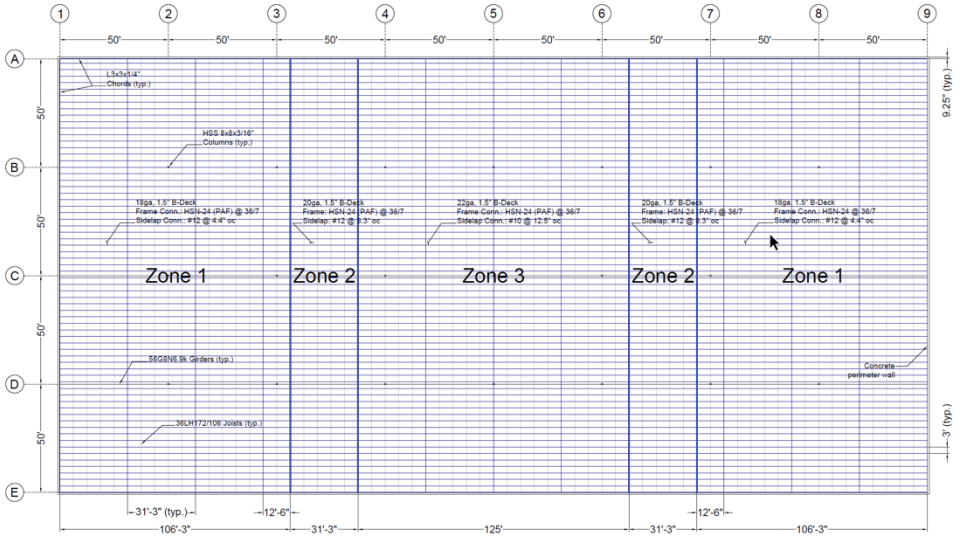

Figure 2: Roof plan view of RWFD steel deck large building archetype (1’ = 0.30 m, 1” = 25.4 mm)

3 MULTI-SCALE MODEL OF RWFD BUILDINGS

A model with sufficient fidelity to capture all key nonlinearities in RWFD buildings and high enough efficiency to be employed across the wide number of seismic excitations required by the incremental dynamic analysis procedures employed in FEMA P695 [16] is desired. Steel deck diaphragms have three dominant sources of nonlinearity in their in-plane shear (diaphragm response): connector nonlinearity, material nonlinearity of the steel, and geometric nonlinearity of the thin-walled deck profile. Including all nonlinearity in a single model would require employing shell elements to model the B deck for the entire 61 m x 122m (200 ft x 400 ft) roof, along with nonlinear elements for all the connectors. This is computationally too expensive.

To meet the fidelity and efficiency needs the multiscale model of Figure 3 has been developed. The roof (deck) nonlinear response is captured phenomenologically as nonlinear hysteretic springs. The hysteretic springs are realized as 1D truss elements at a density set by the panel width and the joist spacing. The roof springs are determined from a 3D roof submodel, which consists of 4 decks in a 5 span condition, the same as in the design. The 3D roof submodel uses shell elements for the decks and nonlinear springs for all the connectors. The nonlinear connectors are based on phenomenological models fit to cyclic shear testing that matches the deck thickness and profile as well the connector details (PAF, screw, weld, etc.). Subsequent sections of this paper explain each of the steps in the modeling and the work conducted to complete each step.

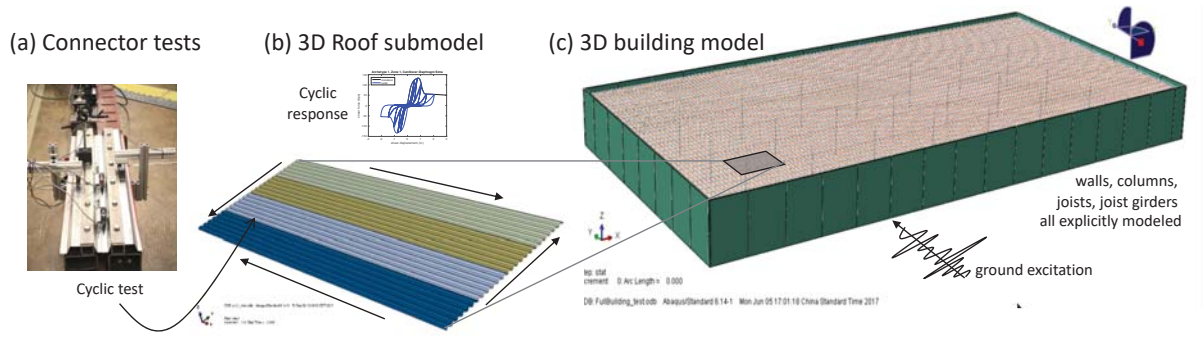

Figure 3: Multiscale RWFD building model

4 CYCLIC CONNECTOR TESTING AND CHARACTERIZATION

4.1 Test setup, test matrix, and cyclic loading protocol

Previous tests on deck-to-deck connectors in shear suffered from unintentional out-of-plane deformations [8] and are limited in scope [4]. A new testing rig was developed to provide the needed data. The testing rig is similar to that prescribed in AISI test standards [17] but modified to further isolate the connector performance by stiffening the deck flutes from deforming (see top clamps in Figure 4a and b) and isolating the shear behavior. The rig consists of a sliding (controlled by a hydraulic actuator) and fixed part – the fixed part is either a second deck in the case of sidelap connections or a 4.76 mm (3/16 in.) steel plate in the case of structural connectors as shown in Figure 4a and b. Two connectors are tested in each specimen.

The connector tests are performed cyclically using the FEMA 461 [18] loading protocol. The loading history consists of two repeated cycles of step-wise increasing deformation amplitude ($a_{i+1}=1.4a_i$) as shown in Figure 4c. The protocol is defined to reach a deformation associated with the most severe damage state at a preset point in the loading protocol, e.g. the 20th cycle was selected. It is also recommended that at least six cycles be completed prior to reaching the lowest damage state, this was also implemented. The protocol is simple and robust and has been used successfully in previous steel-to-steel connector tests [19].

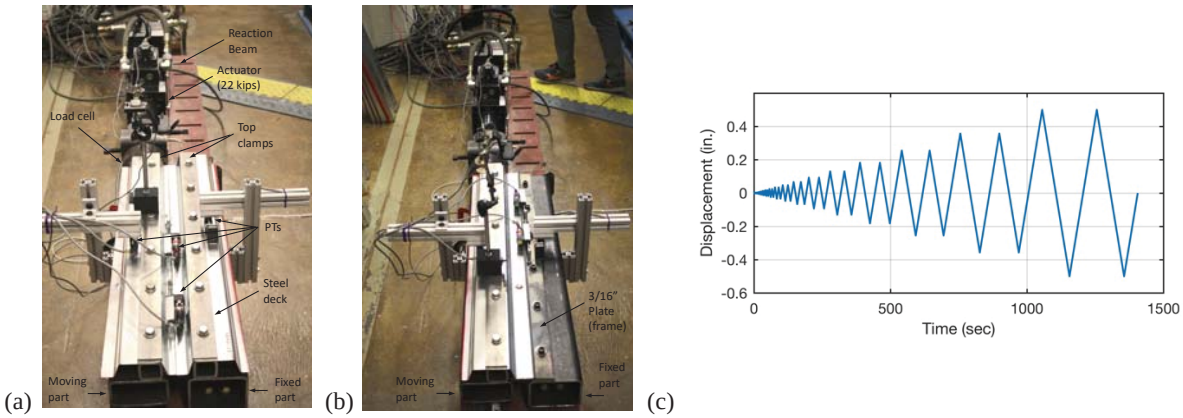

Figure 4: Cyclic shear testing (a) sidelap (b) structural (c) FEMA 461 [18] loading protocol

The tested configurations, totaling 24 sidelap tests and 36 structural tests, are summarized in Table 1. The test matrix is intended to cover non-proprietary deck connection details for U.S. practice both in the East (largely wind controlled) and the West (largely seismic controlled). A number of proprietary systems also exist, particularly for interlock deck. These

systems are not considered here at this time, but the testing and modeling protocols established herein provide a path for their later inclusion.

Table 1: Matrix of tested connectors.

Deck (1.5 in. WR)	Ply 1 (gauge)	Ply 2 (gauge)	Connector	# tests[6] *n*
nestable	18	18	#12 screw	4
nestable	20	20	#12 screw	4
nestable	22	22	#10 screw	4
interlock	18	18	Top Arc Seam Weld[2]	4
interlock	20	20	Top Arc Seam Weld[2]	4
interlock	22	22	Top Arc Seam Weld[2]	4
nestable	18	plate[1]	PAF-Hilti[3]	4
nestable	20	plate[1]	PAF-Hilti[3]	4
nestable	22	plate[1]	PAF-Hilti[3]	4
nestable	18	plate[1]	Arc spot[4]	4
nestable	20	plate[1]	Arc spot[4]	4
nestable	22	plate[1]	Arc spot[4]	4
interlock	18	plate[1]	Arc seam[5]	4
interlock	20	plate[1]	Arc seam[5]	4
interlock	22	plate[1]	Arc seam[5]	4

1. 4.76 mm (3/16 in. plate)
2. 38.1 mm (1.5 in.) long weld
3. HILTI X-HSN 24 PAF
4. visible weld diameter 19 mm (3/4 in.)
5. Visible length 38 mm (1.5 in.), width 9.5 mm (3/8 in.)
6. 1 monotonic and 3 cyclic for each unique condition.

4.2 Performance of deck-to-deck sidelap connector tests

Complete test results are provided in [20]. Sample results for the thinnest tested, 22 gauge, deck is provided in Figure 5. In general, the strength is higher and the ductility slightly reduced in the thicker deck. Significant variability is observed in the screwed sidelap test results. As shown in Figure 5a, the screws are installed close to the web-lip junction and the lip itself is narrow making it challenging to meet edge distance requirements [21]. Depending on the installation tooling used it may be more common to drive the fastener at 90 degrees to the lip and into the flat, or to drive the fastener at an angle into the web-lip corner – both are deemed acceptable in practice [22]. Fasteners installed into the work hardened corners readily meet edge distance requirements, and may result in increased stiffness and strength, but may also have lower ductility.

Top arc seam welds in interlock deck generally have larger strength than screwed sidelaps. With this larger strength comes more dramatic post-peak loss in strength once the weld separates (Figure 5c,d). The typical failure mode of the top arc seam sidelap is shown in Figure 5c. In almost all cases, the failure was not visible from the top side of the specimen because the connection failure occurred at the edge of the “male” steel deck, which is welded to the “female” steel deck in the interlocking sidelap.

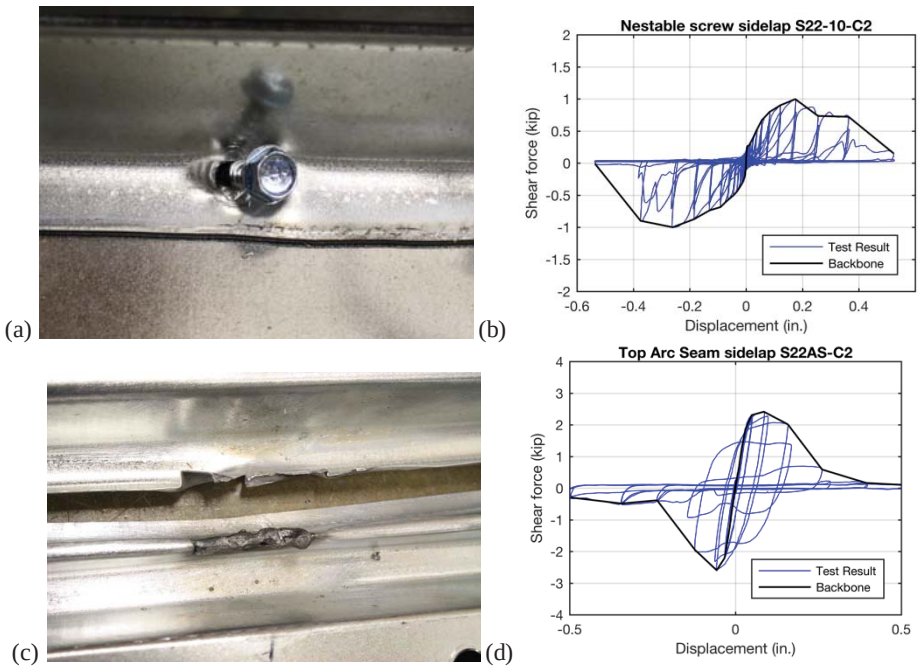

Figure 5: Typical performance of sidelap tests in 22 gauge deck (a) screw tilting and bearing (b) example cyclic performance of single fastener, (c) separation of top arc seam weld in interlock deck at end of test, (d) cyclic performance of single top arc seam weld

4.3 Performance of deck-to-structural connector tests

Roof deck is attached to joists, joist girders, and perimeter chords and collectors. In these cases, the connection is from a relatively thin deck (ply 1) to thicker (typically hot-rolled) steel members. As summarized in Table 1 two classes of connectors are studied: power actuated fasteners (PAFs) and welds. Complete results are provided in [20].

Performance of the PAFs is summarized in Figure 6 – in general the performance is excellent with large capacities and significant and stable post-peak ductility. The ductility gradually reduces in the thinner 22 gauge deck as compared to the thicker deck. As shown in Figure 6a, the damage in the steel sheet is not as favorable for the thinner gauge deck.

Figure 6: Cyclic shear performance of PAF (a) bunching and damage in 22 gauge deck, (b) slotting and tearing in 20 and 18 gauge deck, (c) typical cyclic response of single PAF in 18 gauge deck

Performance of the welds is summarized in Figure 7. The weld connections exhibit high initial stiffness and strength with minimal post-peak ductility. The arc spot welds (Figure 7a) often can only take 1 or fewer cycles post-peak, the arc-seam welds (Figure 7b) perform modestly better. There is typically no residual capacity at large deformations.

Figure 7: Cyclic shear performance of welds (a) arc spot in 20 gauge deck at failure, (b) arc seam in 22 gauge deck at failure, (c) typical cyclic response of single arc spot weld in 20 gauge deck

4.4 Characterization of cyclic connector test results

As depicted in Figure 2 the cyclic connector tests need to be phenomenologically characterized so that connector models may be introduced into the 3D roof submodel. A large variety of options exist for the characterization; however, the one-dimensional "Pinching4" (P4) hysteretic material model developed in [23] has seen wide use for cyclic characterization due to its general nature and implementation in OpenSees [24]. The P4 model includes a 4 point linear segment backbone curve, and unloading, reloading, pinching, and cyclic degradation parameters.

We established the symmetric backbone response by averaging the positive and negative quadrants for each cyclic test sample and taking the minimum of this average across the three cyclic tests. The linear segments are selected so the third point is the peak and the area (energy) under the backbone matches the tests. We established the unloading, reloading, and pinching parameters by minimizing the error in the per cycle energy. Results for a typical screwed sidelap and a PAF structural connection are provided in Figure 8.

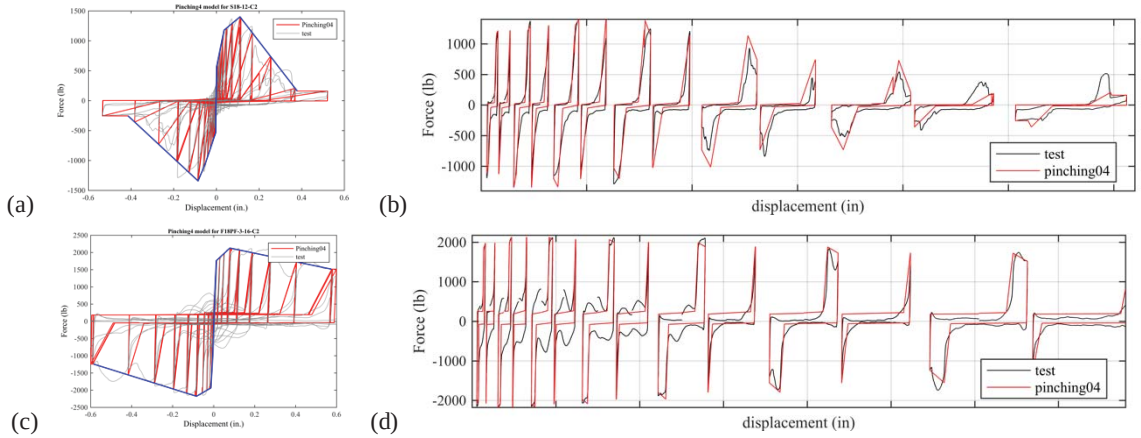

Figure 8: Pinching 4 fit to cyclic shear response (a) nestable screw sidelap in 18 gauge deck (b) per cycle comparison of screwed sidelap (c) PAF in 18 gauge deck (d) per cycle comparison of PAF

5 3D ROOF SUBMODEL SIMULATION AND CHARACTERIZATION

5.1 Modeling details and roof in-plane shear response

The 3D Roof Submodel is essentially a simulation of a cantilever diaphragm test, conducted with details that match the RWFD archetype roof zones, as given in Figure 2. The model is completed in ABAQUS [25] and consists of a pin connected external frame modeled with beam elements, four pin-ended interior joists modeled with beam elements, four 914 mm (36 in.) wide 9.53 m (31 ft 3 in.) long deck panels modeled with shell finite elements, and user defined connector elements that implement the P4 model for the sidelap and structural

connections between the deck panels, and between the deck panels and the frame. A unique feature of the model is the use of P4 user defined elements, as developed in [26], for all connectors. These user elements are calibrated against the connector testing of the previous section. The pin-jointed frame is pinned to ground at the corners of one side, and displaced laterally on the opposite side, as depicted in Figure 9a. The FEMA 461 displacement protocol is enforced for the entire frame and an implicit dynamic solution employed in ABAQUS. Loading rates are pseudo-static, but the large descending branches in the connector elements more readily find equilibrium with the dynamic solvers. The modeling protocol was validated against the cantilever diaphragm testing of [10]. One important detail that was determined in this process is that the connector testing has embedded in its results local plate deformations from the deck – if this is not accounted for then the model is overly soft; therefore, a 4 cm by 4 cm region of the deck at every fastener location was modeled as elastic and stiff.

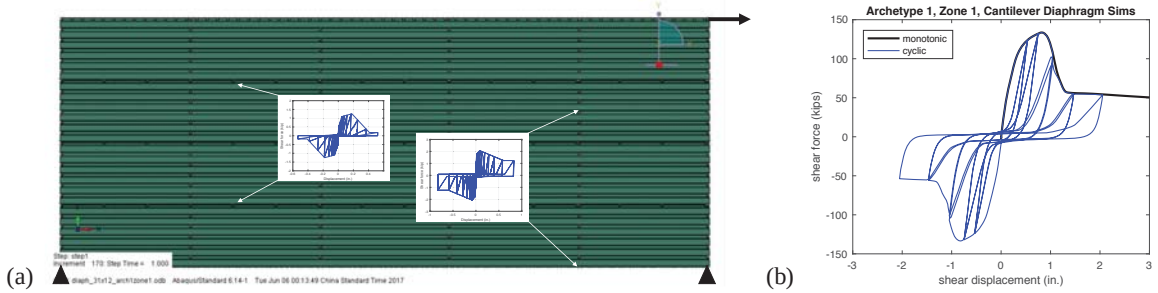

Figure 9: 3D Roof Submodel exercised as a cantilever diaphragm (a) FE model with nonlinear fastener inputs highlighted, and (b) resulting monotonic and cyclic performance for details consistent with Zone 1 of the RWFD building archetype shown in Figure 2

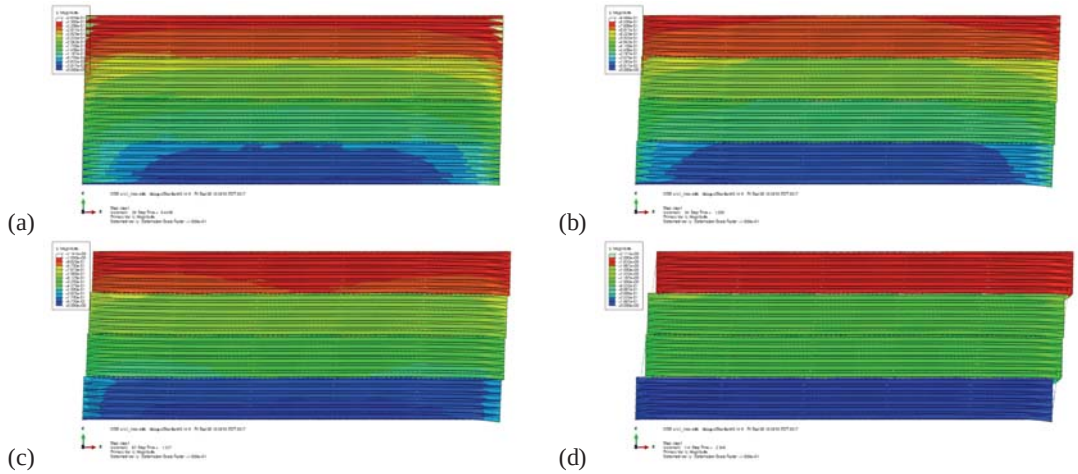

Figure 10: Displacement contours of Zone 1 of RWFD building archetype at (a) 80% pre-peak force, note deck end warping and overall continuity of displacement, (b) peak force, note yielding in deck particularly near corners combined with sidelap failures initiation causes peak, (c) 80% post-peak force, and (d) 40% post-peak force (1.4% drift), note near complete loss of sidelap connection and loss of displacement continuity across the deck.

The resulting shear vs. lateral displacement for the entire roof zone is provided in Figure 9b. Additional models are completed for each roof zone of the RWFD building. The behavior of roof zone 1 of the RWFD building archetype is provided in Figure 9b and 10. Initially the response is linear and uniform across the 4 panels as the sidelaps have sufficient stiffness and capacity to transmit the shear from deck panel to deck panel. Due to the geometry of the deck panels the ends warp creating additional deformations near the member ends (Figure 10a-c),

but local buckling is not observed in the panels. At peak load the sidelaps begin to degrade and the warping has created localized yielding. Past-peak (Figure 10c and d) the sidelaps continue to fail and the stiffness and strength drop to a lower plateau where essentially each panel is independent, but the PAF structural connections between the panel and the joists and panel and the frame provide residual strength.

5.2 Characterization of diaphragm results

Consistent with Figure 2 additional roof submodels must be generated and exercised each time the roof detailing changes. The results across the three designed roof zones of the RWFD building archetype are provided in Figure 11. As the deck gauge is increased and the sidelap and PAF spacing decreased the capacity decreases significantly and a more benign post peak response is observed. For each model the overall response is fit to a new P4 model, one that matches the backbone, unloading, reloading, and pinching parameters of the full 3D roof submodel. This is then converted into P4 user defined elements that can be understood as nonlinear hysteretic 1D "truss" elements – and Figure 11a shows the accuracy of the P4 fitting, and that the "truss" element implementation is correct.

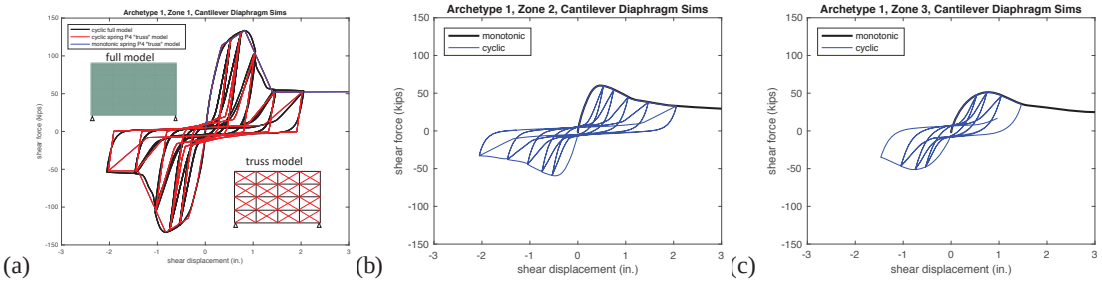

Figure 11: Monotonic and cyclic response for RWFD archetype building roof (a) zone 1, (b) zone 2, (c) zone 3. In (a) roof zone 1 results also show P4 fit and conversion to reduced order roof truss model

6 RWFD BUILDING MODEL AND SIMULATION RESULTS

A complete 3D RWFD building model of the archetype of Figure 2 is developed in ABAQUS. The roof employs the nonlinear "truss" derived from the 3D Roof submodel as shown in Figure 12a for the in-plane shear behavior. The trusses are spaced at a distance equal to the panel deck width (0.9 m or 3 ft) and every supporting joist (1.9 m or 6.25 ft). The trusses are closed off, in the plane of the roof, by pin-ended struts perpendicular to the joists that have an out-of-plane stiffness equal to the effective bending stiffness of the deck. For the steel supporting structure, the HSS columns, joists, and joist girders are all modeled as steel fiber element sections (F_y=345 MPa, 50 ksi) as depicted in Figure 12b. The joists and joist girders are modeled as I-sections with depth and strong and weak axis moment of inertia that match the design sections (36LH176/106 for the joists and 56G8N6.9k for the joist girders). The HSS columns are modeled as a box fiber section of the same dimensions as the design: 203 mm x 203 mm x 4.76 mm (8 in x 8 in x 3/16 in.). The concrete walls are modeled as individual elastic panels with thickness of 235mm (9.25 in.) and height of 10m (33 ft), inclusive of a 0.9 m (3 ft) parapet as shown in Figure 12c. Appropriate density is applied to all elements in the model to properly simulate the mass distribution. The total weight of the building is 24,643 kN (5540 kips). The first step in all models is to initiate gravity and the base reaction in this step equals the design building weight. As described in the following the building model is exercised for vibration analysis, pushover analysis, and scaled nonlinear time history analyses (incremental dynamic analysis).

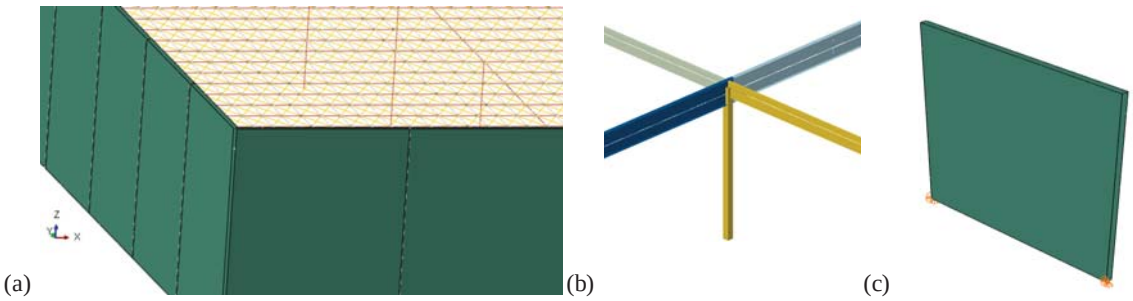

Figure 12: RWFD building model details (a) roof corner (b) representation of joist and joist girder connection on HSS column (c) individual wall panel, pinned at base

6.1 Modal analysis

Modal (vibration) analysis is conducted on the RWFD building archetype and results are summarized in Figure 13 and Table 2 for selected modes. The N-S period of the building is predicted to be 0.59 s and E-W period 0.28 s. This may be compared with the ASCE 7-10 estimated period of 0.26 s which is only a function of building height. FEMA P-1026 [3] provides a new empirical formula for period estimation that is also a function of diaphragm span length and this formula predicts a N-S period of 0.53 s and E-W period of 0.29 s, which is in much better agreement with the developed building model.

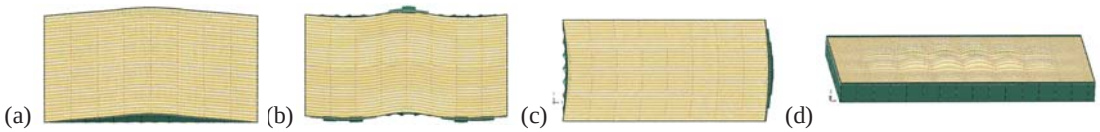

Figure 13: Vibration mode shapes for RWFD building (a) N-S lateral mode 1 (b) N-S lateral mode 2 (c) E-W lateral mode 1, (d) Vertical mode 1

Table 2: Summary modal analysis results

Mode	f	T	M_{eff}	W_{trib}
N-S Lateral (1st)	1.69 Hz	0.59 s	$0.49M_{tot}$	$0.47W_{tot}$
N-S Lateral (2nd)	3.43 Hz	0.29 s	$0.09M_{tot}$	
E-W Lateral (1st)	3.56 Hz	0.28 s	$0.21M_{tot}$	$0.32W_{tot}$
Vertical (1st)	3.31 Hz	0.30 s	$0.07M_{tot}$	$0.17W_{tot}$

The modal effective mass (M_{eff}) provides an estimation of the ratio of the building mass (M_{tot}) which is engaged in a given dynamic mode, and also may be useful for estimating the mass which is tributary to the diaphragm for ELF-based design. As shown in Table 2, the weight tributary to the diaphragm (W_{trib}): taken as the roof weight + the wall weight perpendicular to the motion (i.e., the parapet + ½ the distance to the ground), is roughly similar to the effective mass.

6.2 Nonlinear static analysis

Pushover analysis of the RWFD building archetype is also conducted and summarized in Figure 14. The model is conducted as a quasi-static analysis and solved with implicit dynamics, as this was found to provide more reliable convergence with the large number of softening elements. Material and geometric nonlinearity are included in the model. The applied pushover load is a uniform line load on the walls at the roof diaphragm height. More sophisticated loading profiles are possible and potentially desirable. The peak pushover

capacity is 8038 kN (1807 kips) which may be compared with the nominal design capacity of the roof of 6161 kN (1385 kips) for an overstrength (Ω) of 1.3.

A contour plot of the roof stiffness at peak load is provided in Figure 14b. Each roof zone begins with its own uniform initial stiffness. In regions of higher shear this degrades as larger shear strains are imposed on the roofs. At peak load, approximately 7% of the building width at each end of Zone 1 has experienced substantial reduction in stiffness and when the edge begins to soften (post-peak response) the load carrying capacity of the roof drops suddenly. However, a substantial and stable secondary response is then engaged. This secondary response for Roof Zone 1 is shown in Figure 9b and is based in part on the deformation of the individual sheets once most sidelaps have degraded, Figure 10d, and predicated largely on the benign post-peak response of the PAF structural connectors, Figure 6. In addition, the roof deformations require bending of the joists and joist girders, which also provide secondary resistance.

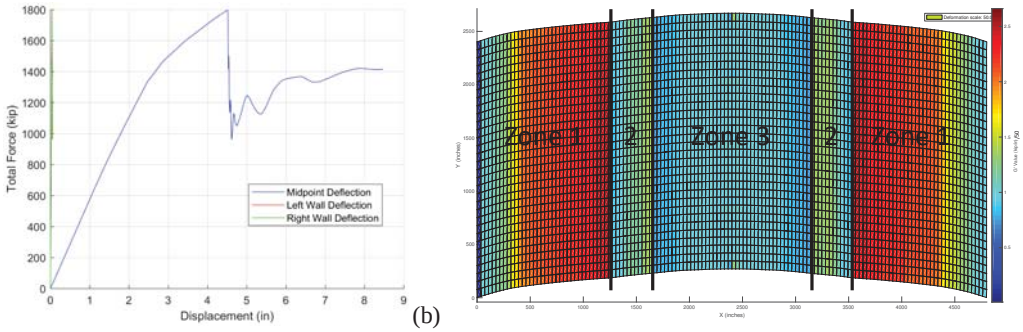

Figure 14: Typical pushover results (a) applied force vs. midpoint roof deflection (b) contour of roof secant stiffness G' at peak load on 50x magnified deformed shape

6.3 Incremental dynamic analyses

FEMA P695 provides a procedure for using suites of scaled nonlinear time history analyses (i.e. incremental dynamic analysis) to establish whether or not seismic response modification coefficients used in ELF seismic design (R, C_d, Ω_o) provide an acceptable probability of collapse. For evaluation in the U.S. FEMA P695 provides a suite of 44 different ground motions to use in the evaluation. Each nonlinear time history analysis is computationally expensive; therefore, a reduced set of motions was selected.

Incremental dynamic analysis in the FEMA P695 evaluation is intended to establish the median collapse margin ratio against the maximum credible earthquake. The RWFD building archetype was designed at a spectral acceleration S_{DS}=1.0g, which implies a maximum credible earthquake demand S_{MT}=1.5g. We ran the 44 P695 earthquake ground motions at $0.5S_{DS}$ (i.e. at a scale factor, SF=0.50) in an effort to find the median 7 EQs that we would explore further. The analysis results are summarized in Figure 15a. The 7 EQ motions that provided roof drift closest to the median of the 44 records were selected for incremental dynamic analyses.

With the 7 selected earthquakes we then ran a series of nonlinear time history analyses scaling the records from $0.5S_{DS}$ up to $3S_{DS}$ and the peak roof drift from each time history is reported in Figure 15. As expected, dispersion in the response increases. The incremental dynamic analysis curves do not indicate an abrupt and nonlinear peak response (large increase in displacements) at the studied demand levels. To determine if building response is acceptable the collapse margin ratio established from the analyses is adjusted based on expected building ductility (by the spectral shape factor, or SSF) and compared with an acceptable collapse margin ratio that heuristically considers the uncertainty of the design

requirements, supporting test-data, and modeling procedure as well as the large uncertainty associated with the ground motions themselves. The acceptable collapse margin ratios (ACMR) are then established for a 20% probability of collapse ($ACMR_{20\%}$) for any given archetype and a 10% probability of collapse for groups of archetypes ($ACMR_{10\%}$). Per FEMA P695 employing a total uncertainty of 0.41 results in an $ACMR_{20\%}$ of 1.56 and $ACMR_{10\%}$ of 1.96. Based on the pushover analysis a ductility of 1.28 is established resulting in a SSF of 1.07, again per FEMA P695. For the design to be considered acceptable the collapse margin ratio, which is S_T/S_{MT} adjusted (multiplied) by the SSF must be greater than $ACMR_{10\%}$ for an individual archetype or $ACMR_{20\%}$ for a group. These values may be readily visualized in the incremental dynamic analysis results as horizontal scale factors that the median building must have successful performance at for the design to be adequate. As Figure 15b shows the median building must have adequate performance at S_T=2.19g for a predicted MCE collapse probability of 20% and S_T=2.75g for 10% probability of collapse. Therefore, to explore the building response in detail we select the median earthquake at SF=2.25g, which is above the acceptable collapse margin for an individual archetype.

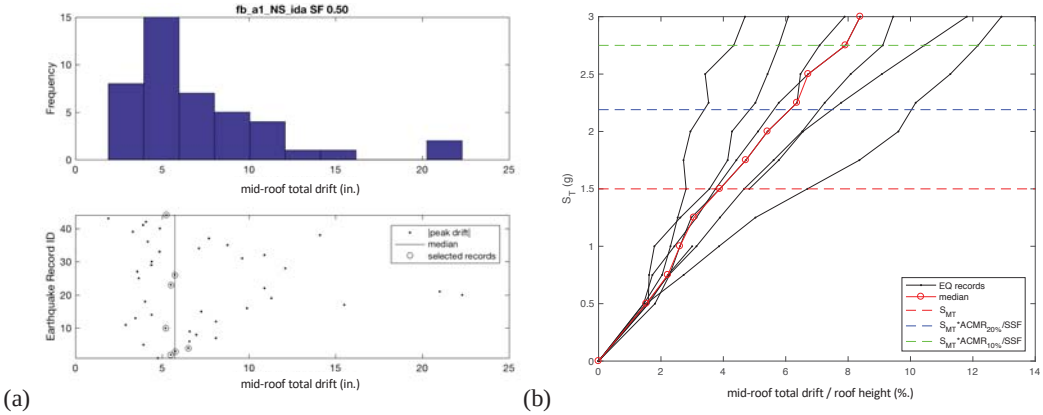

(a) (b)

Figure 15: Peak drift from time history analyses (a) selection of 7 median EQ records from the 44 record P695 suite at a scale factor of 0.50 (b) incremental dynamic analysis results

6.4 Median nonlinear time history response at SF=2.25

The nonlinear time history response of the RWFD building archetype under FEMA P695 earthquake motion 4 at a scale factor (SF) of 2.25 is detailed in this section. The design criteria are considered potentially acceptable if the building has adequate performance at this design level, for this earthquake. The overall building time history response is summarized in Figure 16. The peak base shear, as shown in Figure 16a, of 18200 kN (4100 kips) is greatly in excess of the pushover strength of the roof (8038 kN or 1807 kips). The building period, Figure 16b, substantially elongates during the course of the record, to as large as 2 s. Overall the force-deformation response indicates significant energy dissipation, Figure 16c. The peak force and peak drift occur at different times in the record and both are selected for further investigation.

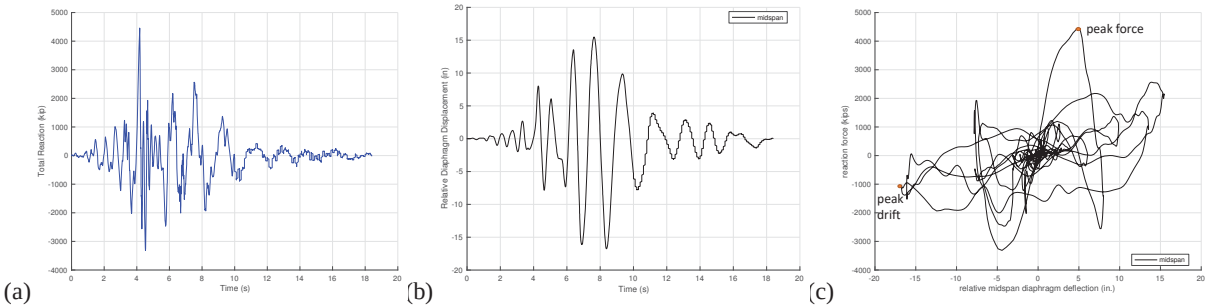

Figure 16: Building response for SF=2.25, FEMA P695 Earthquake 4 (a) base shear in time (b) diaphragm drift in time (c) roof drift vs. base shear over time of response

Similar to Figure 14b, we may explore the degrading roof stiffness to understand how damage propagates through the roof in time. Early in the time history, at the peak force in the response, the roof stiffness degrades at each roof zone transition (Figure 17a). The most significant roof stiffness reductions are at the roof edges (at the region of maximum shear), and the response is quite similar to the pushover peak force response. At peak drift, as shown in Figure 17b, the roof response is more complex. The building exhibits localized response that changes across each zone transition. Significant portions of Roof Zone 1 and 2 have undergone large deformations and are well into their post-peak response. Fully ¼ of the building roof has been significantly damaged. However, secondary load paths in the model, as discussed in the post-peak pushover response, have allowed the building to "survive" without roof displacements increasing without bound (note shape of overall curve in Figure 15b).

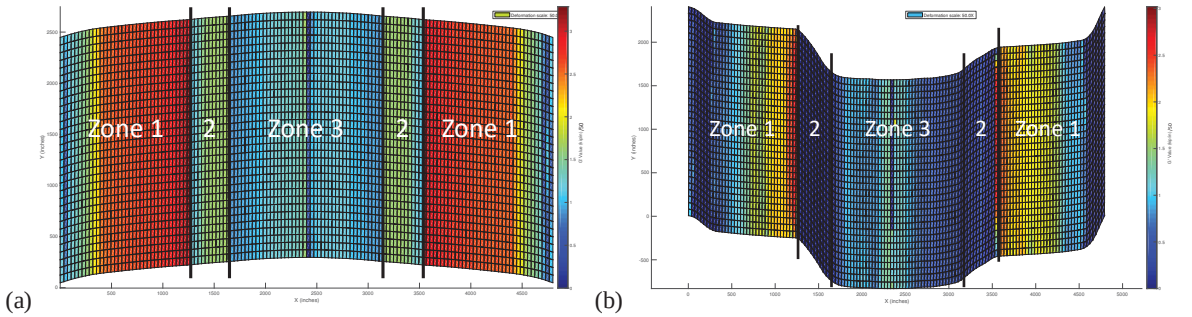

Figure 17: Roof response for SF=2.25, FEMA P695 Earthquake 4, contours of roof secant stiffness G' (a) at peak force in record, and (b) at peak drift in record

In addition to exploring the roof stiffness we may consider the forces that develop in the roof. In particular, the anchorage forces between the roof and walls are of interest. Figure 18a provides the shear distribution for the roof as determined from the anchorage forces at the time in the response coincident with the peak force (base shear) in the model. The response is close to the deep beam assumption typically used in design. The collected shear at the end walls at the roof level (9.1m or 30 ft up) is 5053 kN (1136 kips). This may be compared with the dynamic base shear (ground level) at the end walls which is 18238 kN (4100 kips) at the same moment in time. Thus, the peak diaphragm force demand is 28% of the base shear demand, significantly less than even the tributary assumptions or effective mass of Table 2. Also note, while the base shear is more than double the pushover strength the diaphragm level shears remain less than the pushover capacity. Only a small portion of the mass is engaged and carried by the roof diaphragm as most of the mass is in the walls, not the roof, for these systems. As a result, the diaphragm level demands are significantly less than the base shear demands. This is a unique feature of RWFD buildings with heavy walls.

At peak drift, once the roof is damaged, the simple linear variation in shear at the roof level is not observed. The individual anchorage forces are provided in Figure 18b and they indicate significant demands in the corners and large concentration of anchorage demands in regions where the roof is heavily degraded. These anchorage forces deserve further study as they can provide further insight on the secondary load paths that are engaged for the damaged roof and may inform anchorage design requirements.

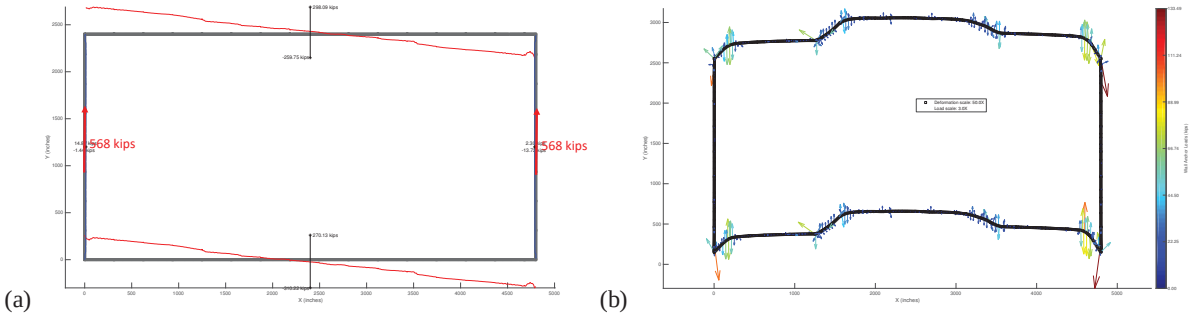

Figure 18: Roof response for SF=2.25, FEMA P695 Earthquake 4, examination of in-plane forces (a) summation of anchorage force and distribution at peak force in record, and (b) vector plot of individual anchor forces at peak drift in record

7 FUTURE WORK AND DISCUSSION

Significant future work remains to provide a complete evaluation of RWFD buildings with thin-walled steel deck as the primary roof diaphragm element. Additional analysis of the anchorage forces and secondary load paths that exist in the currently studied model may help illuminate these secondary systems and provide means to capacity protect some elements if necessary.

Examination of an RWFD building with more modest seismic demands and that employ details more consistent with wind-controlled designs may provide different results. Consideration of other roof connectors, particularly welds, in the RWFD building modeling is needed. Even though the initial analysis appears to indicate adequate performance for ASCE 7-10 based design, evaluation of the proposed FEMA P-1026 procedure, which requires different detailing of the roof zones and uses different procedures for estimating the demands is still needed.

A complete analysis of the RWFD building archetype in the E-W direction was performed. The response was essentially elastic with no to little damage up through scale factors consistent with even the 10% collapse probability. FEMA P695 provides evaluation procedures for 3D models under two-way excitation. It may be useful to explore excitation in two directions to determine if the whole building response is improved or degraded, and if there is benefit to exercising the full model as opposed to separating into two motions.

Additional connector testing, both on systems in past use (e.g. button punched sidelaps) and the variety of proprietary connectors now used would be beneficial. Further exploration of the performance of endlaps and related connectors in the 3D Roof Submodel could also be beneficial. Endlaps potentially provide increased stiffness as opposed to the free edges explored here, but they also provide potential locations of stiffness change similar to roof zone transitions and can place unique demands on connectors. All of which are worthy of further study. The work reported here was conducted by NBM Technologies. The first author is now continuing the work as an unfunded effort under the Cold-Formed Steel Research Consortium.

8 CONCLUSIONS

The seismic behavior of Rigid Wall Flexible Diaphragm (RWFD) buildings is unique. Heavy concrete walls are often paired with light roof diaphragm systems and the response deviates from typical seismic building design assumptions. Building upon significant prior work in the literature a model is developed for thin-walled steel deck roof diaphragms that incorporates key nonlinearities; including, nonlinear hysteretic response at deck-to-deck and deck-to-structural connections, material and geometric nonlinearity of the deck itself, and the inclusion of secondary load paths including post-peak response after the failure of deck-to-deck connections. Experiments are conducted and reported for establishing the nonlinear connector performance. A shell finite element model is developed for the roof that captures the key nonlinearities. The roof results are then embedded in a larger building model which includes discrete models for the walls, columns, joists, joist, girders, anchorage, and roof. A large RWFD building archetype is designed per current U.S. procedures and evaluated in a method similar to FEMA P695, i.e., through performing incremental dynamic analyses. The results indicate that the building design is potentially adequate, but this conclusion relies on significant damage in the roof and the activation of a number of secondary load paths. Further, the model indicates that a smaller percentage of the building shear is carried through the diaphragm than typically assumed. Additional work is needed to fully investigate RWFD building performance, provide definitive guidance with respect to proposed alternative design procedures, and develop improved seismic design details to limit the damage to the roof.

ACKNOWLEDGMENTS

The work reported herein was conducted by NBM Technologies for the American Iron and Steel Institute, Steel Deck Institute, and Steel Joist Institute. An Industry Steering Group consisting of Patrick Bodwell, James Fisher, Thomas Sputo, Bob Paul, Ken Charles, Dave Samuelson, and Bonnie Manley provided regular feedback on the work. Patrick Bodwell's support in building archetype design is recognized herein and was instrumental to completing the archetype model. In addition, a peer review team managed by the Applied Technology Council and chaired by Dominic Kelly, with participation from John Lawson, Robert Tremblay, Mai Tong, Kelly Cobeen, and Veronica Cedillos has provided regular feedback. Any opinions, findings, and conclusions or recommendations expressed in this material are those of the authors and do not necessarily reflect the views of the sponsors or other industry participants.

REFERENCES

[1] Koliou, M., Filiatrault, A., Kelly, D. J., & Lawson, J. (2016). Buildings with rigid walls and flexible roof diaphragms. I: Evaluation of current U.S. seismic provisions. *Journal of Structural Engineering, 142*(3)10.1061/(ASCE)ST.1943-541X.0001438

[2] Koliou, M., Filiatrault, A., Kelly, D. J., & Lawson, J. (2016). Buildings with rigid walls and flexible roof diaphragms. II: Evaluation of a new seismic design approach based on distributed diaphragm yielding. *Journal of Structural Engineering, 142*(3)10.1061/(ASCE)ST.1943-541X.0001439

[3] FEMA (2015). Seismic Design of Rigid Wall-Flexible Diaphragm Buildings: An Alternate Procedure (FEMA P-1026). Federal Emergency Management Agency. access at https://www.fema.gov/media-library/assets/documents/105764

[4] Koliou, M., & Filiatrault, A. (2017). Development of wood and steel diaphragm hysteretic connector database for performance-based earthquake engineering. *Bulletin of Earthquake Engineering, 15*(10), 4319-4347. 10.1007/s10518-017-0141-7
[5] Koliou, M. (2014). "Seismic Analysis and Design of Rigid Wall – Flexible Diaphragm Buildings." Ph.D. Dissertation, University at Buffalo, State University of New York.
[6] O'Brien, P., Eatherton, M.R., Easterling, W.S. (2017). "Characterizing the load-deformation behavior of steel deck diaphragms using past test data." CFSRC Report 2017-02. access at http://jhir.library.jhu.edu/handle/1774.2/40633
[7] Tremblay, R., & Stiemer, S. F. (1996). Seismic behavior of single-storey steel structures with a flexible roof diaphragm. *aian Journal of Civil Engineering, 23*(1), 49-62. 10.1139/l96-006
[8] Rogers, C. A., & Tremblay, R. (2003). Inelastic seismic response of side lap fasteners for steel roof deck diaphragms. *Journal of Structural Engineering, 129*(12), 1637-1646. 10.1061/(ASCE)0733-9445(2003)129:12(1637)
[9] Rogers, C. A., & Tremblay, R. (2003). Inelastic seismic response of frame fasteners for steel roof deck diaphragms. *Journal of Structural Engineering, 129*(12), 1647-1657. 10.1061/(ASCE)0733-9445(2003)129:12(1647)
[10] Essa, H. S., Tremblay, R., & Rogers, C. A. (2003). Behavior of roof deck diaphragms under quasistatic cyclic loading. *Journal of Structural Engineering, 129*(12), 1658-1666. 10.1061/(ASCE)0733-9445(2003)129:12(1658)
[11] Tremblay, R., Martin, E., Yang, W., & Rogers, C. A. (2004). Analysis, testing and design of steel roof deck diaphragms for ductile earthquake resistance. *Journal of Earthquake Engineering, 8*(5), 775-816. 10.1142/S1363246904001699
[12] ASCE (2016). *Minimum Design Loads and Associated Criteria for Buildings and Other Structures*. American Society of Civil Engineers. ASCE/SEI 7-16, ISBN (print): 9780784414248ISBN (PDF): 9780784479964
[13] ASCE (2010). *Minimum Design Loads for Buildings and Other Structures*. American Society of Civil Engineers. ASCE/SEI 7-16, ISBN (print): 9780784412916ISBN (PDF): 9780784477854
[14] AISI (2013). AISI S310-13, *North American Standard for the Design of Profiled Steel Diaphragm Panels.* American Iron and Steel Institute, Washington DC.
[15] ACI (2011). *Building Code Requirements for Structural Concrete and Commentary*. ACI 318-11. American Concrete Institute.
[16] FEMA (2009). *Quantification of Building Seismic Performance Factors.* FEMA P695. Federal Emergency Management Agency.
[17] AISI (2014). *Test standard for cold-formed steel connections*. AISI S905-14. American Iron and Steel Institute, Washington DC.
[18] FEMA (2007). *Interim Testing Protocols for Determining the Seismic Performance Characteristics of Structural and Nonstructural Components*. FEMA 461. access at https://www.fema.gov/media-library/assets/documents/15207
[19] Tao, F., Chatterjee, A., Moen, C.D. (2017). "Monotonic and Cyclic Response of Single Shear Cold-Formed Steel to Steel and Sheathing-to-Steel Connections." *AISI RP17-2.* American Iron and Steel Institute.
[20] Torabian, S., Schafer, B.W. (2017). "Cyclic performance and characterization of steel deck connections." *Technical Report* to American Iron and Steel Institute, Steel Deck Institute, and Steel Joist Institute (available upon request).
[21] AISI (2016) *North American Specification for the Design of Cold-Formed Steel Structural Members*. AISI S100-16. American Iron and Steel Institute.
[22] SDI (2015) *Diaphragm Design Manual*, 4th Ed., Steel Deck Institute.
[23] Lowes, L. N., Mitra, N., and Altoontash, A. (2004). A Beam-Column Joint Model for Simulating the Earthquake Response of Reinforced Concrete Frames. *PEER Report* 2003/10 access at http://peer.berkeley.edu/publications/peer_reports/reports_2003/0310.pdf

[24] McKenna, F., Scott, M.H., and Fenves, G.L. (2010). "Nonlinear Finite Element Analysis Software Architecture Using Object Composition." *Journal of Computing in Civil Engineering*, 24(1):95-107, January 2010.
[25] ABAQUS (2014). *ABAQUS/Standard User's Manual*, Version 6.14. Providence, RI: Simulia.
[26] Ding, C. (2015). “Monotonic and Cyclic Simulation of Screw - Fastened Connections for Cold - Formed Steel Framing.” Virginia Polytechnic Institute and State University. MS Thesis. access at http://hdl.handle.net/10919/55270